Analytical Methods

Colorimetric detection of catalase and catalase-positive bacteria (E. coli) using silver nanoprisms

Colorimetric detection of catalase and catalase-positive bacteria (*E. coli*) using silver nanoprisms

Lili Zhao, Julia Wiebe, Rabia Zahoor, Sladjana Slavkovic, Brian Malile, Philip E. Johnson and

Jennifer I. L. Chen*

Department of Chemistry, York University, 4700 Keele Street, Toronto, ON, Canada M3J 1P3

*E-mail: jilchen@yorku.ca

KEYWORDS: colorimetric detection, pathogen, Ag nanoprisms, *E. coli*, catalase, plasmonics, food safety.

ABSTRACT

Portable, cost-effective and rapid sensing methods are desirable in areas such as environmental monitoring, food safety and point-of-care diagnostics. Colorimetric signals arising from plasmonic nanoparticles have been widely explored for the detection of biomarkers, ions and small molecules, but to a less extent for pathogens such as bacteria. Herein we explore the innate sensitivity of the formation of silver nanoprisms to hydrogen peroxide as a means to detect catalase activity, which is present in various bacteria associated with foodborne illnesses. The formation of large silver nanoprisms with plasmon resonance at long wavelengths is facilitated by the oxidative etching of the nanoparticles in the presence of a reducing agent and citrate. When enzymes such as catalase disrupts this redox balance, the morphology and size of the particles change to yield a color shift from blue to purple, red, orange and yellow. We show

that the multi-color transition of Ag colloidal solutions can provide quantification of catalase and

E. coli by eye in the range of $0 - 0.1$ U and $10^6 - 10^7$ cfu/mL (corresponding to $0.01 - 0.1$ pM),

respectively. We demonstrate the ability to detect *E. coli* on artificially contaminated lettuce leaf.

When combined with pre-concentration and purification techniques, the visual readout may be

useful for on-site analysis and monitoring of food and water quality.

INTRODUCTION

Pathogens are a global issue and their detection is important for health and safety reasons.

Despite advances in sanitation and technology for identifying and controlling infectious diseases,

pathogens are still prevalent with the main problems lying within the food industry. In addition,

recurring incidents of bacterial contaminations in water and their potential use in bioterrorism

make pathogen detection an important issue.

Conventional pathogen detection methods such as colony counting, polymerase chain

reaction (PCR), and immunology-based assays are well established.[1] Despite the ability to

provide reliable and unambiguous results, colony counting is time consuming, while methods

such as PCR and immunology-based assays require several intermediate steps and rely on

expensive and sophisticated instruments. These characteristics limit application outside of

specialized laboratories. Electrochemical-based detection offers some advantages including low

detection limit,[2-4] but generally require tagged probe molecules and instrumentations. Hence,

considerable effort has been directed towards developing simple, rapid, inexpensive and portable

sensing platforms.[5, 6] Qualitative and quantitative detection of bacteria can be achieved by

monitoring enzymatic activities such as catalase, β-glucuronidase[7] or β-galactosidase[8] in

Escherichia coli. Catalase is a ubiquitous enzyme that protects cells from oxidative damage by

decomposing hydrogen peroxide to water and oxygen.[9] It is found in various bacteria including *E. coli*, *Salmonella* and *Listeria*, which contribute to major foodborne illnesses. Decomposition of H_2O_2 by catalase gives rise to the foaming activity that can be visualized and semi-quantitative,[10] while the conversion of chromogenic molecules by β-galactosidase or β-glucuronidase can yield colorimetric response on a paper strip.[5] Because the chromogenic compounds generally yield an intensity change and the magnitude of which, if small, may be challenging to discern by eye, alternative methods to produce a broad range of colors across the detection range are desirable.

Plasmonic noble nanoparticles exhibit localized surface plasmon resonance (LSPR) in the visible wavelengths, the energy of which can be tuned by controlling the size and shape of the particles[11, 12], as well as through interparticle coupling.[13-15] These colloidal solutions have therefore been applied to a plethora of colorimetric sensing applications. Anisotropic nanoparticles, such as prisms[12, 16] and rods[17], offer the synthetic flexibility to tune the LSPR from visible to the IR wavelengths and therefore are ideal candidates for deriving a broad range of colorimetric response. Recently changes in the morphology of these particles have been explored for the targeted detection of small molecules[18-20], gluocose[21, 22], biomarkers[23] and bacteria.[24] The colorimetric response arises either from etching of the particles or enzymatic-induced deposition of additional metal on the colloidal nanoparticles. In some works, the need to label or chemically modify the probe molecules is completely circumvented[18, 19, 21, 22], while in others, high sensitivity with ultralow detection limit have been demonstrated.[23, 24]

Herein we explore the sensitivity of the formation of silver nanoprisms to hydrogen peroxide as a means to detect catalase activity. We show the multi-color transition of Ag colloidal solutions synthesized with different concentrations of catalase and *E. coli*. When

combined with pre-concentration and purification techniques, the semi-quantitative readout of the concentrations may be useful in resource-limited settings or on-site analysis without instrumentation.

EXPERIMENTAL

Materials. Silver nitrate (99.9999%), sodium citrate dihydrate (≥99%,), sodium borohydride (≥99%) and polyvinylpyrrolidone (PVP, weight-average MW ~ 29,000 g/mol) and bovine liver catalase (2000 – 5000 units/mg) were purchased from Sigma Aldrich. Hydrogen peroxide (30 wt%,) was purchased from EMD. Glycerol stock of *Escherichia coli* was provided by Dr. Golemi-Kotra and *Streptococcus salivarius* was purchased from Pulse Scientific (Microbiologics ATCC 19258 Lyfodisk). Reagents for cell culturing including Bacto-tryptone, bacto-yeast extract, sodium chloride and sodium hydroxide were purchased from BioShop Canada. Brain heart infusion broth and agar plates were purchased from Hardy Diagnostics. Water used was deionized to 18 MΩ with Millipore filtration system and autoclaved for cell cultures.

Synthesis of Ag Nanoprisms. Preparation of the silver nanoprisms was modified from the literature method and carried out in a 96-well plate. In a typical procedure, $AgNO_3$ (1 mM, 25 μL), citrate (30 mM, 15 μL), PVP (0.35 mM, 10 μL) were pipetted into the wells. A solution of H_2O_2 (71 mM, confirmed via absorbance at 240 nm) was added in decreasing volumes across the wells 1-12 (100, 80, 60, 40, 35, 30, 25, 20, 15, 10, 5 and 0 μL), respectively. Additional volumes of water were added accordingly to bring each well to an equal volume. A volume of 70 μL of freshly prepared $NaBH_4$ (1.2 mM) was then added to each of the wells. The total volume of the synthesis was 220 μL. Color changes were observed after the reactions proceeded for 10-20 minutes.

4

Synthesis of Ag Nanoprisms with Catalase. A catalase solution of 1 mg/mL was prepared in water and its activity determined by monitoring the decomposition rate of H_2O_2 using UV-vis spectrophotometer. The stock solution (5540 U/mL) was diluted for use in the Ag synthesis. A volume of 60 μL H_2O_2 (71 mM,) was added to each well followed by the addition of 20 μL of catalase of various concentrations (0, 0.2, 0.4, 0.8, 1.0, 1.2, 1.5 and 1.8 U). The final concentration of catalase in the reactions was 7.8 to 70.8 nM of the tetramer. The mixture of H_2O_2 and catalase in each well was allowed to react for 5 minutes. Additional volumes of water were added to bring each well to an equal volume. The rest of the reagents, $AgNO_3$ (1 mM, 25 μL), citrate (30 mM, 15 μL) and PVP (0.35 mM, 10 μL), were added and a volume of 70 μL of 1.2 mM $NaBH_4$ was injected lastly to obtain the color development. For desalting and purification, Bio-Rad bio-spin columns were used.

Culture of *Escherichia. coli*. *E.coli* strain BL21 (DE3) containing an empty pET 24a vector was provided by Dr Golemi-Kotra's research lab (York University). Transformed colonies were grown in 5 mL of LB media with 5 μL of 10 mg/mL kanamycin overnight at 200 rpm and 37°C. A volume of 200 μL of production cultures were further grown in 50 mL of LB media supplemented with 50 μL 10 mg/mL kanamycin at 37°C until OD_{600} reached 0.8. The culture was divided into 1.5 mL fractions and cell pellets collected by centrifugation at 6500×g for 4 minutes using IEC Micromax tabletop centrifuge. The cells were rinsed twice with autoclaved water.

Culture of *Streptococcus Salivarius*. *S. salivarius* pellet was rehydrated using 1.0 mL of Brain Heart Infusion Broth (BHIB). This aliquot was then aseptically transferred to the BHIB containing culture plate and incubated at 37°C for 24h. Colonies were grown in 5 mL of BHIB media overnight at 200 rpm and 37°C. A volume of 0.1 mL of seed culture was transferred to 25

5

mL of BHIB. Growth was continued at 37°C to an OD_{600} of 0.6. The culture was divided into 1.5 mL fractions and cell pellets were collected by centrifugation at 6500×g for 4 minutes using IEC Micromax tabletop centrifuge. The cells were rinsed three times with autoclaved water.

Colony counting of *E. coli.* The purified *E. coli* pellet was diluted with autoclaved water to an OD_{600} of 1.09. A volume of 0.1 mL of *E. coli* diluted by factors ranging from 10^0 to 10^9 with 0.9% NaCl was added to separate LB agar plates containing 30 µL of 10 mg/mL kanamycin and incubated at 37 °C for 24 hours. The numbers of colonies (not exceeding 100) on the petri dishes were counted. The concentration of fresh *E. coli* culture was determined to be 7.9 x 10^8 cfu/mL, close to the reported literature value.[25]

Synthesis of Ag Nanoprisms with *E. coli* and *S. salivarius*. A volume of 20 µL of *E. coli* in varying quantities (0, 1.05, 2.03, 3.58, 5.07, 6.84 and 8.96×10^8 cfu/mL) was added to each well with H_2O_2 initially and other reagents for Ag synthesis were injected after 5 minutes. For the synthesis of Ag nanoparticles with control bacteria, a volume of 20 µL of *S. salivarius* in varying quantities with comparable OD to *E. coli* was added. Color changes were observed after the reactions proceeded for 10-20 min.

Real sample test. Fresh lettuce was purchased from a local grocery store. A piece of the lettuce (3×9 cm) was dipped in 35 mL of *E. coli* solution (OD_{600} = 1.074) for 10 min, removed and dried in the air for 1 h. The lettuce was rinsed with 10 mL of autoclaved water and the recovered *E. coli* solution was centrifuged at $6500 \times$ g for 15 min. The supernatant was removed to concentrate the solution 100 times for use in the Ag synthesis.

Characterization. UV-Vis spectra of samples in 96-well plate were measured using BioTek Synergy H4 Hybrid. A Varian Cary 100 UV-vis spectrophotometer was used for measuring

bacteria OD, catalase activity and H_2O_2 stock solution. The morphology of nanoparticles was characterized using Transmission Electronic Microscopy (TEM, Philips EM201). The images were analyzed using the software ImageJ to quantify particle size and size distribution.

RESULTS AND DISCUSSION

The synthesis of silver nanoprisms was adapted from a previous work.[26] The thermal synthesis route is versatile for tailoring the morphology of the nanoprisms. It relies on the reduction of silver ions by $NaBH_4$ in the presence of capping ligands such as citrate and PVP to prevent particle aggregation. The oxidative etchant, H_2O_2, establishes a redox equilibrium and drives shape selection. By adjusting the amounts of the reducing and oxidizing agents in the reaction, the ratio of nanoprism edge length to thickness and corner truncations vary and thereby controlling the wavelength of the LSPR peak. Figure 1a shows a photograph of the silver nanoparticles prepared by varying the concentration of H_2O_2 while keeping all other reagent concentrations constant. As the concentration of H_2O_2 decreased from 32.3 to 0 mM, the color of the resulting silver nanoparticles changed from blue to purple, light red and yellow, suggesting changes in the size and shape of the silver nanoparticles. Figure 1b shows the UV-vis spectra corresponding to each well. At 32.3 mM of H_2O_2, the extinction spectrum shows a strong in-plane dipole plasmon mode of the nanoprism at ~600 nm. Two smaller peaks at 337 nm and 400 nm are also observed – they correspond to the in-plane and out-of-plane quadrupole modes respectively.[27] As the concentration of H_2O_2 decreases, the main LSPR peak blue shifts and the extinction near 400 nm increases, suggesting the formation of small Ag spherical seeds instead of prisms. We calculate the intensity ratio of the LSPR in-plane dipole mode of prisms vs that of the spheres (400 nm) as a means to monitor the changes in the morphology of the particles. Figure 1c summarizes the dominant LSPR peak wavelength, and the intensity ratio of prism to

spheres as a function of H_2O_2 concentration. The intensity ratio decreases from 2.84±0.37 for >13 mM of H_2O_2 to 0.87±0.29 for 3.2 mM of H_2O_2. Both the extinction spectra and the colorimetric image show the high sensitivity of the nanoprism formation to the H_2O_2 concentration. Note that the errors shown in Fig. 1c are standard deviations of three runs, demonstrating the reproducibility of the synthesis when carried out in parallel. Additional experiments show that the range of colors can be tuned by varying sodium borohydride and silver nitrate, and the reaction time can be shortened by eliminating PVP (Fig. S1). The high sensitivity of the resultant LSPR to the reaction condition requires careful preparation of the reagents, and some variability may arise due to changes in the activity of sodium borohydride. The broad range of colors derived from plasmonic Ag nanoparticles allows for semi-quantitative detection of H_2O_2 by eye, in contrast to the binary colors of H_2O_2-induced aggregation of Au nanoparticles.[28, 29]
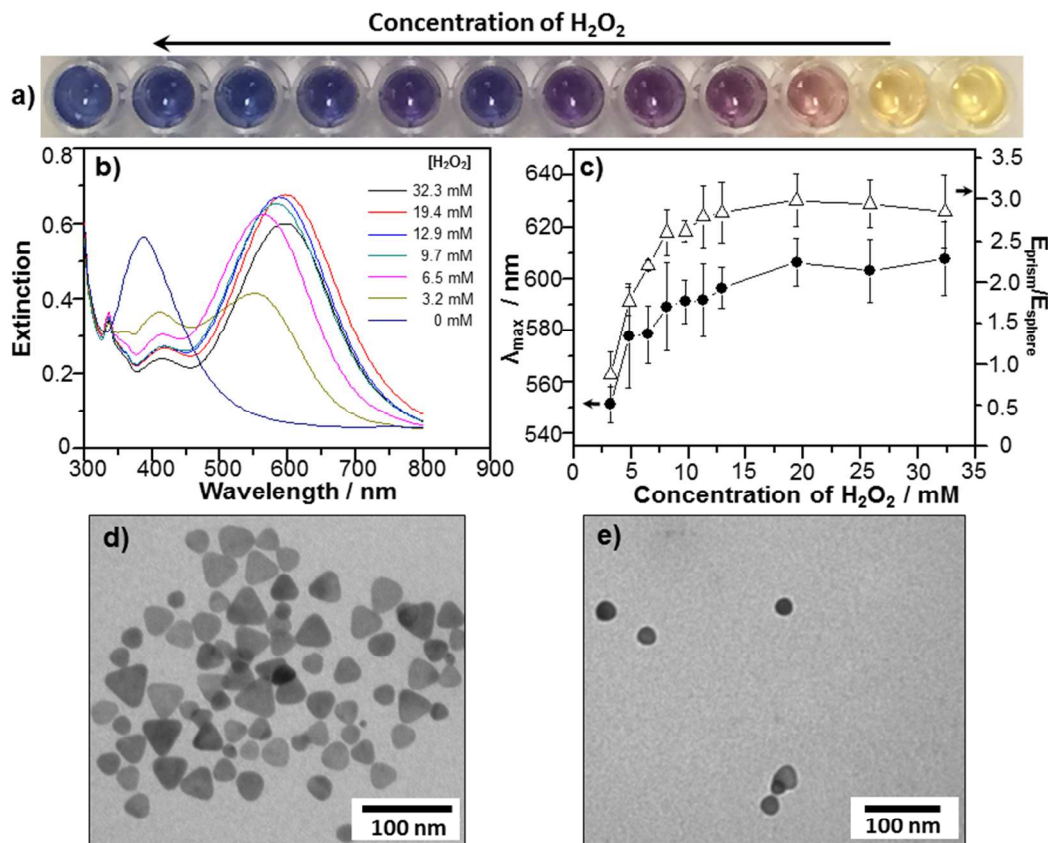
Figure 1. Photograph (a) and extinction spectra (b) of silver nanoparticles synthesized by changing the concentration of H_2O_2. Trends in the dominant LSPR peak wavelength and intensity ratio of prisms to spheres with respect to the concentration of H_2O_2 (c). TEM images of silver nanoparticles synthesized at 32.3 mM (d) and 3.2 mM (e) of H_2O_2. The errors are standard deviation of three runs.

Nanoparticle morphologies were further characterized using TEM. Figure 1d and e show

the TEM images of particles synthesized at 32.3 mM and 3.2 mM of H_2O_2. We categorized the

shapes as prisms and spheres and analyzed their size distribution (Fig. S2). At 3.2 mM of H_2O_2,

we observe a high ratio of spheres to prisms with spherical particles accounting for 73% of the

total. In contrast at 32.3 mM of H_2O_2, 65% of the particles were found to be well defined

nanoprisms. These results corroborate that morphological changes in the nanoparticles give rise

to changes in the extinction spectra and the broad range of colors. The sensitivity of the silver

nanoparticle synthesis to H_2O_2 therefore can be exploited for the detection of enzymes or

pathogens that catalyze its decomposition.

Next we explore the detection of catalase, a common enzyme that catalyzes the decomposition of hydrogen peroxide to water and oxygen, using the Ag synthesis. We set all of the solutions to contain the same initial concentration of H_2O_2 (19.4 mM) and added different amounts of catalase. Figure 2a shows the photograph of the Ag nanoparticle solutions synthesized with increasing amount of catalase (0 to 0.16 U) demonstrating the colorimetric response. As the catalase activity increases from 0 to 0.16 U, the colors of the obtained silver nanoparticles show similar transition to that of the original synthesis with decreasing concentration of H_2O_2. Without catalase, the concentration of H_2O_2 remains high and nanoprisms were formed to give the blue color of the solution. At high catalase activity (0.11 to 0.16 U), hydrogen peroxide decomposed significantly and no anisotropic particles were obtained; as a result the solutions are yellow. Figure 2b shows the extinction spectra of the solutions and Figure 2c summarizes the changes in the dominant LSPR peak wavelengths and intensity ratios of prism
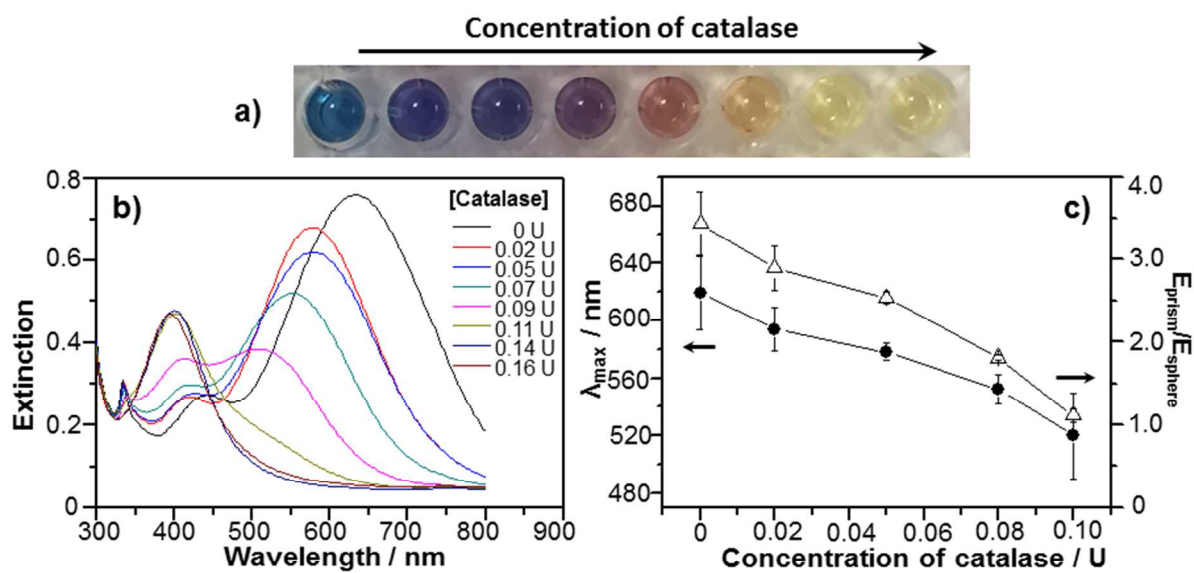
Figure 2. Photograph (a) and extinction spectra (b) of the silver nanoparticle solutions synthesized with different concentrations of catalase. Trends in the dominant LSPR peak wavelength and intensity ratio of prisms to spheres with respect to the catalase concentration (c). The errors are standard deviation of three runs.

to spheres for different concentrations of catalase. The trends mirror that of the original Ag synthesis with LSPR peaks shifting from 619±25 nm to 520±30 nm and finally 400 nm, and intensity ratio decreasing from 2.44±0.38 to 1.11±0.08, and finally ~0 when only spheres were produced.

We carried out several control experiments to elucidate the role of catalase on the Ag synthesis. First, we examined other possible effects of proteins on the Ag synthesis by using bovine serum albumin (BSA, Sigma Aldrich) instead of catalase. Solutions of BSA with similar concentrations (in mg/mL) as catalase were used in the Ag synthesis. No obvious changes in the color and extinction spectra were observed (Fig. S3). This result supports that the color transition seen with catalase in the reaction (Fig. 2) arises from the enzymatic decomposition of H_2O_2 rather than non-specific interaction of protein with the nanoparticles. We also studied the effect of catalase and BSA on pre-synthesized silver nanoprisms as some researchers have noted the

possibility of proteins altering the morphology or stability of nanoparticles post-synthetically.[30]

The as-prepared silver nanoprisms were mixed with different concentrations of catalase and BSA.

Again, negligible change was observed for both the color and extinction spectra (Fig. S4),

indicating that catalase and BSA do not affect the size and shape of the pre-synthesized silver

nanoprisms. Thus we conclude that catalase affects the reaction conditions of the Ag synthesis

by decomposing H_2O_2.

Because the formation and stability of Ag nanoprisms are highly sensitive to reaction

conditions, purification steps may be required to remove interferences such as halides. Figure S5

shows the adverse effects of chloride and phosphate ions on the colorimetric response, in which

the anions prevented the formation of Ag nanoprisms. The ions, however, can be readily

separated from proteins by size-exclusion spin columns, and the detection of catalase in the

presence of these ions is possible (Fig. S5b). The application of Ag nanoprisms for colorimetric

sensing of complex samples may be feasible by employing purification or extraction methods

such as size exclusion columns, immune-capturing beads, or microfluidics. Furthermore, the use

of alternative stable reducing agent would be desirable for field applications.

We apply the colorimetric detection scheme to catalase-positive bacteria, *E. coli*. Figure

3a shows the photograph of the Ag solutions containing increasing amount of *E. coli*; the color

changes from blue to purple, pink and colorless, suggesting the decomposition of hydrogen

peroxide by the bacteria. The concentration of *E. coli* examined is in the range of OD_{600} of 0.011

to 0.095, which translates to 0.013 to 0.11 pM (or 1.9×10^6 to 1.6×10^7 cells in the reactions) and

0.88×10^7 to 8.1×10^7 cfu/mL from our colony count. The corresponding extinction spectra are

shown in Figure 3c. With increasing concentration of *E. coli* up to 4.6×10^7 cfu/mL, the LSPR

peak wavelength shifts from 640 to 478 nm and the intensity ratio decreased from 2.73 to 1.36; the LSPR peak completely disappears at the highest amounts of *E. coli* tested. The data are summarized in Fig. 3d and the trends are within that of the catalase experiment except colorless solutions were produced with high amount of *E. coli*. We observed that the bacteria do not have to be viable to exhibit catalase activity: When we tested out *E. coli*. that had been stored in the freezer (1270 cfu/mL compared to 7.9×10^8 cfu/mL per OD for fresh culture), we obtained similar color transition from blue to orange (Fig. S6). So long as the catalase activity is present, the colorimetric response may be achieved.
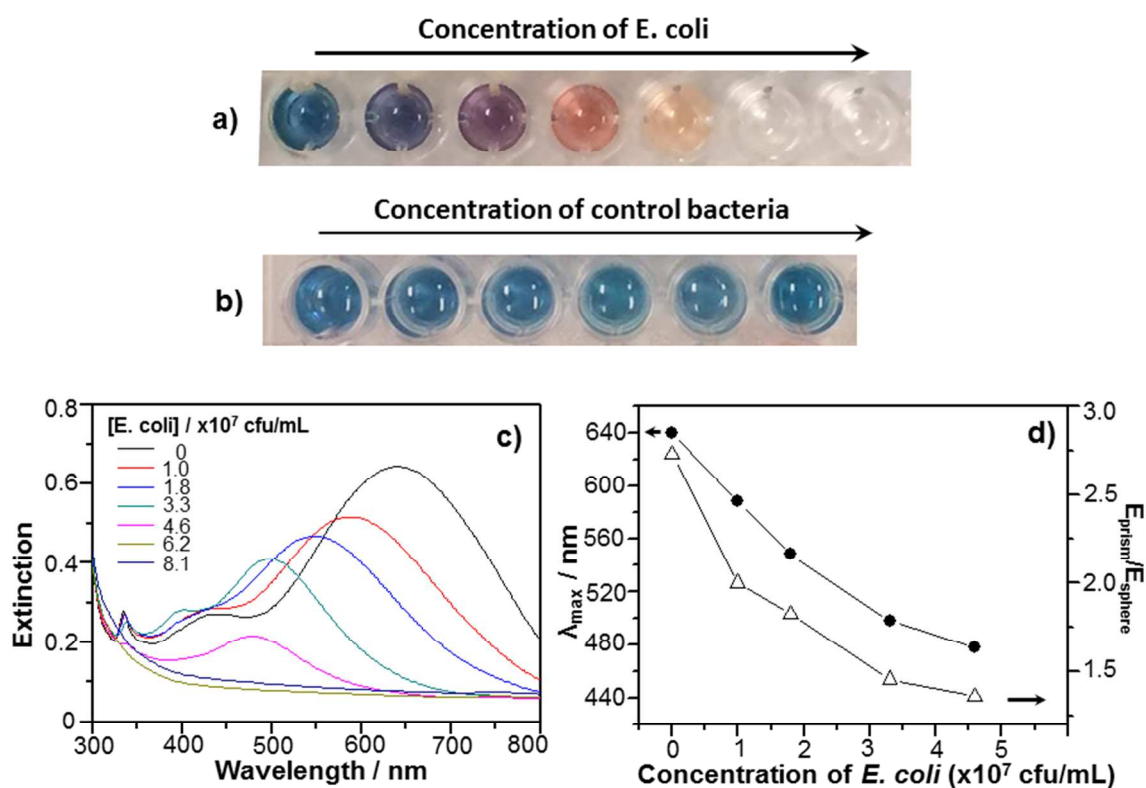
Figure 3. Photographs of silver nanoprisms synthesized with *E. coli* (a) and *S. salivarius* (b) of different concentrations. The optical densities of the *E. coli* and the control bacteria were similar (0 to 0.05). Extinction spectra and trends in the dominant LSPR peak wavelength and intensity ratio with respect to the concentration of *E. coli* are shown in (c) and (d), respectively.

As a control experiment, we synthesized the Ag particles with a catalase-negative bacterium - *Streptococcus salivarius*. The solutions all appear blue with increasing concentration of *S. salivarius* (Fig. 3b, see Fig. S7 for spectral information). The effect of *E. coli* on pre-synthesized silver nanoprisms was also studied. We observed negligible changes in the color and extinction spectra when *E. coli* was added to the pre-synthesized particles (Fig. S8). Thus we can rule out other bacteria-induced effects, and confirm that the influence on the size and shape of the silver nanoparticles is achieved through the catalytic decomposition of hydrogen peroxide.

Lastly we demonstrate the potential of colorimetrically detecting *E. coli* in contaminated food as a real world scenario. Fresh lettuce was purchased from a local grocery store and artificially contaminated with *E. coli*. The recovered *E. coli* was concentrated and the solution was used for the synthesis of silver nanoparticles. Water was used in the control experiment. As shown in Figure 4, the silver nanoparticles synthesized with the recovered solution of *E. coli*-contaminated lettuce exhibits purple color while the control solution is blue. Both the spectral and visual difference suggests the potential of this detection platform for monitoring food safety. While the sensing platform is promising, we observed some differences in the colorimetric response in this test which likely arose from variations in the recovery efficiency of *E coli* on the lettuce leaves. Further development of this methodology to include capture macromolecules, such   as   antibodies   or
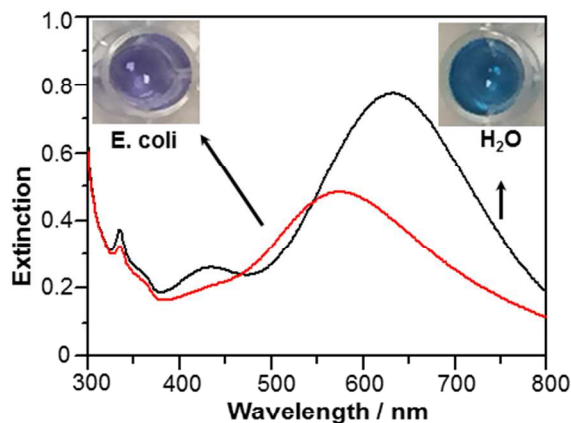
Figure 4. Extinction spectra of the silver nanoparticle solutions synthesized with recovered *E. coli* from contaminated lettuce and H_2O as control. Corresponding photographs of the solutions are shown in the inset.

aptamers, to concentrate and purify bacteria would be desirable as well as providing specificity

and increased sensitivity.

CONCLUSIONS

In summary, we demonstrate the colorimetric detection of catalase activity based on the

synthesis of silver nanoprisms. The LSPR of the colloidal solutions shifts from ~620 nm to 400

nm with increasing amounts of catalase, which correlates with changes in the nanoparticle

morphology. The colorimetric readout spans one order of magnitude in the detection range and

provides the basis for the relative quantification of *E. coli*. Control studies with catalase-negative

bacteria and pre-synthesized nanoparticles suggest negligible non-enzymatic effects. The

applicability of the methodology may be enhanced when combined with pre-purification or

concentration steps that would allow the extraction of bacteria and elimination of interference

species from complex food or biological samples.

ACKNOWLEDGMENTS

1
2
3
4
5
6
7
8
9
10
11
12
13
14
15
16
17
18
19
20
21
22
23
24
25
26
27
28
29
30
31
32
33
34
35
36
37
38
39
40
41
42
43
44
45
46
47
48
49
50
51
52
53
54
55
56
57
58
59
60

Supporting Information. Electronic Supplementary Information (ESI) available. See

DOI: 10.1039/b000000x

REFERENCES

1. O. Lazcka, F. J. Del Campo and F. X. Munoz, *Biosensors & Bioelectronics*, 2007, **22**, 1205-1217.
2. M. Giovanni, M. I. Setyawati, C. Y. Tay, H. Qian, W. S. Kuan and D. T. Leong, *Adv Funct Mater*, 2015, **25**, 3840-3846.
3. Y. Guo, Y. Wang, S. Liu, J. Yu, H. Wang, M. Cui and J. Huang, *Analyst*, 2015, **140**, 551-559.
4. L. Sepunaru, K. Tschulik, C. Batchelor-McAuley, R. Gavish and R. G. Compton, *Biomaterials Science*, 2015, **3**, 816-820.
5. S. M. Z. Hossain, C. Ozimok, C. Sicard, S. D. Aguirre, M. M. Ali, Y. F. Li and J. D. Brennan, *Anal. Bioanal. Chem*, 2012, **403**, 1567-1576.
6. D. A. Giljohann and C. A. Mirkin, *Nature*, 2009, **462**, 461-464.
7. G. J. Delisle and A. Ley, *J. Clin. Microbiol.*, 1989, **27**, 778-779.
8. S. Ratnam, S. B. March, R. Ahmed, G. S. Bezanson and S. Kasatiya, *J. Clin. Microbiol.*, 1988, **26**, 2006-2012.
9. P. Nicholls, I. Fita and P. C. Loewen, in *Advances in Inorganic Chemistry*, Academic Press, 2000, vol. Volume 51, pp. 51-106.
10. T. Iwase, A. Tajima, S. Sugimoto, K. Okuda, I. Hironaka, Y. Kamata, K. Takada and Y. Mizunoe, *Sci Rep-Uk*, 2013, **3**, 3081.
11. Y. Xia, Y. Xiong, B. Lim and S. E. Skrabalak, *Angew. Chem. Int. Ed.*, 2009, **48**, 60-103.
12. R. C. Jin, Y. W. Cao, C. A. Mirkin, K. L. Kelly, G. C. Schatz and J. G. Zheng, *Science*, 2001, **294**, 1901-1903.
13. P. Nordlander, C. Oubre, E. Prodan, K. Li and M. I. Stockman, *Nano Lett.*, 2004, **4**, 899-903.
14. J. Liu and Y. Lu, *Angew. Chem. Int. Ed.*, 2006, **45**, 90-94.
15. C. Sonnichsen, B. M. Reinhard, J. Liphardt and A. P. Alivisatos, *Nature Biotech.*, 2005, **23**, 741-745.
16. J. E. Millstone, S. J. Hurst, G. S. Metraux, J. I. Cutler and C. A. Mirkin, *Small*, 2009, **5**, 646-664.
17. B. Nikoobakht and M. A. El-Sayed, *Chem. Mater.*, 2003, **15**, 1957-1962.
18. B. Malile and J. I. L. Chen, *J. Am. Chem. Soc.*, 2013, **135**, 16042-16045.
19. B. Malile and J. I. L. Chen, *Analyst*, 2016.
20. M. Coronado-Puchau, L. Saa, M. Grzelczak, V. Pavlov and L. M. Liz-Marzán, *Nano Today*, 2013, **8**, 461-468.
21. X. Liu, S. Zhang, P. Tan, J. Zhou, Y. Huang, Z. Nie and S. Yao, *Chem Commun*, 2013, **49**, 1856-1858.
22. Y. Xia, J. Ye, K. Tan, J. Wang and G. Yang, *Anal. Chem.*, 2013, **85**, 6241-6247.
23. L. Rodríguez-Lorenzo, R. de la Rica, R. A. Álvarez-Puebla, L. M. Liz-Marzán and M. M. Stevens, *Nat Mater*, 2012, **11**, 604-607.
24. J. Chen, A. A. Jackson, V. M. Rotello and S. R. Nugen, *Small*, 2016, **12**, 2469-2475.
25. J. A. Myers, B. S. Curtis and W. R. Curtis, *BMC Biophysics*, 2013, **6**, 1-16.
26. G. S. Metraux and C. A. Mirkin, *Adv. Mater.*, 2005, **17**, 412-+.
27. P. Yang, H. Portalès and M.-P. Pileni, *J. Phys. Chem. C*, 2009, **113**, 11597-11604.
28. R. de la Rica and M. M. Stevens, *Nat. Nanotechnol.*, 2012, **7**, 821-824.

29. R. de la Rica and M. M. Stevens, *Nat. Protocols*, 2013, **8**, 1759-1764.
30. D. Li, Y. Dong, B. Li, Y. Wu, K. Wang and S. Zhang, *Analyst*, 2015, **140**, 7672-7677.

1
2
3
4
5
6
7
8
9
10
11
12
13
14
15
16
17
18
19
20
21
22
23
24
25
26
27
28
29
30
31
32
33
34
35
36
37
38
39
40
41
42
43
44
45
46
47
48
49
50
51
52
53
54
55
56
57
58
59
60

H_2O_2

$H_2O + O_2$

Ag^+

Concentration

Catalase pos. bacteria

Catalase neg. bacteria

34x12mm (300 x 300 DPI)